2024 IEEE/RSJ International Conference on Intelligent Robots and Systems (IROS)
October 14-18, 2024. Abu Dhabi, UAE

Torque Ripple Reduction in Quasi-Direct Drive Motors Through Angle-Based Repetitive Learning Observer and Model Predictive Torque Controller

Hefei Zhang, Xiaohu Zhang, Jinyu Cheng, Jiangtao Hu, Chao Ji, Yu Wang, Yutong Jiang, Zhen Han, Wei Gao and Shiwu Zhang

***Abstract*— Torque ripple reduction in quasi-direct drive (QDD) motors is crucial in their robotic applications for dynamic locomotion and dexterous manipulation. In this paper, we present a novel approach for reducing torque ripples of QDD motors, which integrates an angle-based repetitive learning observer (ARLO) and a model predictive control-based field-oriented controller (MPC-FOC). The proposed method successfully improves the torque loop control bandwidth and surpasses conventional proportional-integral (PI) controllers owing to the integrated physical constraints inside MPC. Additionally, the ARLO portion is able to mitigate ripple caused by the inherent cogging torque in brushless motors and also the periodic friction torque from the planetary gearboxes in QDD systems. The effectiveness of the proposed method is demonstrated through both simulation of a single QDD motor and experiments on a two-degree-of-freedom robotic leg, where the performance improvement can be 72.7% in speed tracking and 58.5% in trajectory tracking. The proposed method shows great potential in facilitating smooth motion and precise force control in future robotic applications.**

I. INTRODUCTION

Quasi-direct drive (QDD) motors, distinguished by their high torque density, superior control bandwidth and transparent torque feedback, have been prevalent in robotic applications, notably within quadrupedal and bipedal humanoid robots [1], [2], [3], [4]. However, these motors are usually cost-effective brushless direct current (BLDC) motors that exhibit non-sinusoidal electromotive force and considerable cogging torque [5], which are detrimental to achieving smooth position control and precise force control. Additionally, the manufacturing inconsistency of the integrated low-ratio planetary gearboxes inside QDD motors may also lead to axis misalignment and preload forces, resulting in friction torque that is hard to model and compensate due to nonlinearity. As a result, the cogging torque and the friction torque can both cause periodic torque ripple as the motor output shaft rotates, which can further cause either speed fluctuations and thus vibrations and noises at high speeds, or discrete movements or even a halt at low speeds. Torque ripple is acknowledged as a significant challenge in robotic applications of QDD motors [6].

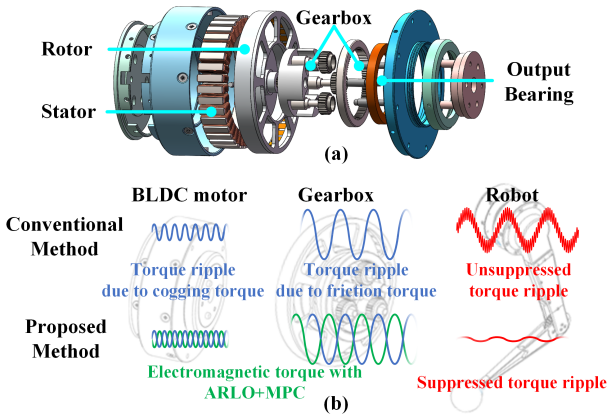

Fig. 1: Overview. (a) The exploded view of a quasi-direct drive motor for robotic joint. (b) The schematics of the torque ripple reduction in quasi-direct drive motors.

Therefore, minimizing torque ripple is critical for robots equipped with QDD motors to accomplish diverse tasks [7]. However, not too much work has been done that takes the cogging torque and the friction torque into consideration at the same time. There are generally two approaches to reduce torque ripple. The first involves innovative motor design [8], such as optimizing pole-slot count, skewing stator lamination and rotor magnetization [9], using higher precision position sensing and improving gearbox manufacturing tolerance [10]. However, the increased manufacturing cost resulted from this approach is against the initial intention of using cost-effective motors in robotic applications. The second approach involves suppressing the torque ripple through control algorithms inside the motor driver, which has become feasible owing to the improved computation power of the onboard microcontroller [11] and is adopted in this work.

Previously, torque ripple in direct drive motors has been

This work was supported in part by the National Natural Science Foundation of China under Grants 62103395, U21A20119 and U22B2040 and in part by the Chinese Scholartree Ridge State Key Lab under the open grant. (Hefei Zhang and Xiaohu Zhang are co-first authors.) (Corresponding authors: Wei Gao; Shiwu Zhang.)

Hefei Zhang and Jiangtao Hu are with the Institute of Advanced Technology, University of Science and Technology of China, Hefei, Anhui 230088, China.

Xiaohu Zhang, Jinyu Cheng, Chao Ji, Wei Gao and Shiwu Zhang are with the Department of Precision Machinery and Precision Instrumentation, College of Engineering Science, University of Science and Technology of China, Hefei, Anhui 230027, China, and Chao Ji is also with the iFLYTEK Co., Ltd., Hefei, Anhui 230088, China. weigao@ustc.edu.cn; swzhang@ustc.edu.cn

Yu Wang is with the School of Mechanical Engineering and Automation, Harbin Institute of Technology Shenzhen, Shenzhen, Guangdong 518055, China.

Yutong Jiang and Zhen Han are with the Chinese Scholartree Ridge State Key Lab, Fengtai, Beijing 100072, China.

effectively dealt with through feeding corresponding compensation current forward to the controller based on a pre-measured torque ripple lookup table [6]. This method has managed to suppress the impact of motor cogging torque to speed control, and has been widely adopted in robotic applications via the open-source controller ODrive. However, this method is not optimal for QDD motors that have built-in reduction gears because it is incapable of online identification of the variable cogging torque and friction torque.

Within the context of online identificaiton, resonant controllers are adept at suppressing periodic ripple, but they exhibit limited effectiveness against disturbances under unknown variable frequencies [12], [13]. Meanwhile, disturbance observers can monitor variation of loads and friction forces under unknown frequencies in real time [14], but their limited bandwidth renders them inadequate for tracking high-frequency disturbances like the cogging torque. On the contrary, repetitive controllers [15] and iterative learning [16] can learn the desired suppression input by iteratively refining it to reduce the torque ripple. They are flexible to variable disturbance frequencies. However, existing research primarily focuses on direct drive motors, overlooking the torque ripple caused by frictions in the gearbox of QDD motors. Besides, considering the limited computation resource of the onboard microcontroller, a modified version of repetitive controller is utilized in this work.

Additionally, the speed PI controller employed by the traditional Field-Oriented Control (FOC) scheme in QDD motors has constrained bandwidth. Torque ripple induced by the cogging torque occurs at much higher frequencies than that of the stator's base electrical cycle, making FOC ineffective in dealing with such high frequency inputs. This limitation can lead to appreciable amplitude attenuation and phase delay when regulating alternating disturbances like the cogging torque, even at reduced speeds [17]. Conversely, Model Predictive Control (MPC) can provide enhanced dynamic response, improved nonlinearity handling and better constraint management [18], [19], making it ideal for accurate current tracking and effective torque ripple reduction.

Therefore, this work proposes a novel control method to reduce both electromagnetic and mechanical torque ripple in QDD motors without any extra torque sensor. The method incorporates an angle-based repetitive learning observer (ARLO) to address the electromagnetic cogging torque and the gearbox-related friction torque. Additionally, an MPC-based field-oriented controller (MPC-FOC) is utilized to overcome the bandwidth limitation of traditional PI-based field-oriented controller (PI-FOC) and realize more effective torque ripple minimization through a customized cost function. As a result, the proposed method can alleviate torque ripple of QDD motors in robotic applications through cascaded online observation and suppression.

The remainder of the paper first introduces the QDD motor model and the torque ripple reduction scheme in Section II, and then delves into the model predictive torque controller and the angle-based repetitive learning observer in Section III. Section IV discusses the corresponding simulation and experimental results, and finally Section V concludes the paper.

II. QDD MOTOR MODEL AND TORQUE RIPPLE REDUCTION SCHEME

A. QDD Motor Model

An exploded view of the QDD motor studied in this paper can be found in Fig. 1(a). The motor consists of three major components: a rotor with 21 pairs of surface-mounted permanent magnets, a stator with fractional slot concentrated winding and a planetary gearbox. Besides the iron core, the stator also has support structures and a driver board. The planetary gearbox is embedded among the stator coils to minimize the motor volume. With a reduction ratio of 6:1, the gearbox presents effective torque magnification and transmission transparency. As illustrated in Fig. 1(b), traditional motor control methodologies do not account for the cogging and friction torques, resulting in complex torque ripple at the output end. This is carefully considered in the following model development.

Typically, a surface-mounted permanent magnet motor can be mathematically modeled with vector control in the dq-coordinate system as

$$\begin{cases} u_d = Ri_d + L_d\frac{\mathrm{d}i_d}{\mathrm{d}t} - \omega_e L_q i_q, \\ u_q = Ri_q + L_q\frac{\mathrm{d}i_q}{\mathrm{d}t} + \omega_e(L_d i_d + \psi_f), \end{cases} \tag{1}$$

where the subscript d and q represent the d-axis and the q-axis, respectively, u, i and L are the corresponding stator voltage, current and inductance, respectively, R is the stator phase resistance, ω_e is the electrical angular velocity, and ψ_f is the magnet flux linkage. Consequently, the electromagnetic torque T_e generated by the motor can be derived as

$$T_\mathrm{e} = \frac{3p}{2}[\psi_f i_q + (L_d - L_q) i_d i_q], \tag{2}$$

where p is the number of pole pairs. Because the vector control fixes i_d to zero, T_e can be rewritten as

$$T_\mathrm{e} = \frac{3p}{2}\psi_f i_q \tag{3}$$

The cogging torque is primarily associated with the motor's design and exists regardless of whether or not there is current in the coils. The direction and magnitude of the cogging torque vary with the rotor's angular position. Therefore, the mathematical model for the cogging torque can be expressed as

$$\begin{aligned} T_{cogg} = \sum_{k=1}^{n} [&T_{k,\sin}\sin(k\cdot \mathrm{LCM}(Q,2p)\cdot\theta_m) + \\ &T_{k,\cos}\cos(k\cdot \mathrm{LCM}(Q,2p)\cdot\theta_m)], \end{aligned} \tag{4}$$

where $T_{k,\sin}$ and $T_{k,\cos}$ denote the amplitudes of the k-th harmonic component of the sinusoidal and cosinusoidal elements, respectively, $\mathrm{LCM}(Q,2p)$ represents the least common multiple of the slot number Q and the pole pair number $2p$, and θ_m indicates the angle of the rotor on the motor side.

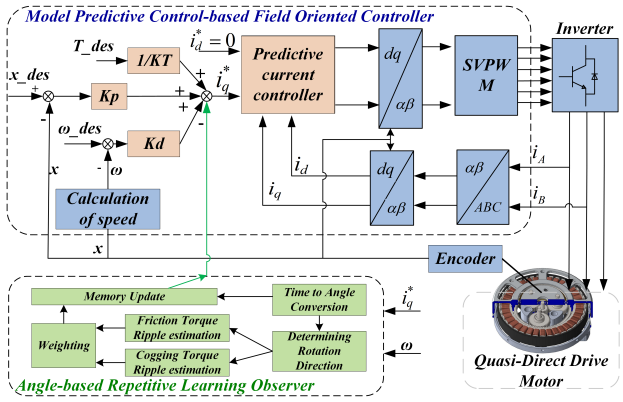

Fig. 2: Control system schematics of torque ripple reduction in QDD motors.

The friction torque generated by misalignment in motor gearbox exhibits periodicity relative to the decelerated angle, which can be modeled as

$$T_{fr} = \mathcal{T}_{fr}(\theta_l), \tag{5}$$

where $\theta_l = \theta_m / N_{rat}$ represents the rotor angle on the load side.

B. Torque Ripple Reduction Scheme

As depicted in Fig. 2, the overall motor driver with torque ripple suppression functionality incorporates an angle-based repetitive learning observer and an MPC-based field-oriented controller. The observer takes advantage of the motor's position and current sensors to observe the cogging and friction torques. No additional sensors are needed. It then takes algorithmic and sensor delays into consideration and sends the torque ripple compensation current to the controller. In the meantime, the motor employs the proportional control scheme commonly used in legged robots to control its position and speed, thus the desired signal for the current control loop within the controller can be calculated. The controller also samples the three-phase stator currents from the motor and transforms them to the dq-coordinate system for feedback current control. The current controller then uses the MPC algorithm to track the desired current within a control cycle, thereby avoiding torque undershoot or overshoot and realizing high-bandwidth torque control. Note that the output of the MPC algorithm are desired voltages in the dq-coordinate system for the motor, which are transformed into the three-phase duty cycle of the inverter by Space Vector Pulse Width Modulation to enhance voltage utilization within the driver. The goal is to generate a desired motor torque that can counteract the motor's torque ripple as illustrated in Fig. 1(b).

III. TORQUE RIPPLE REDUCTION METHOD

A. Model Predictive Control-based Field-oriented Controller

The limitation of traditional PI torque control lies in overlooking current and torque limits during transient phases. To address it, this study employs a continuous-set MPC framework that incorporates motor current limit constraints. This approach ensures that current limits are adhered to, thereby preventing torque overshoot and undershoot.

Based on (1), the MPC problem can be formulated as

$$\begin{cases} \mathbf{x}(k+1) = \mathbf{A}_c\mathbf{x}(k) + \mathbf{B}_c\mathbf{u}(k) + \mathbf{G}_c v(k), \\ \mathbf{y}(k) = \mathbf{C}_c\mathbf{x}(k), \end{cases} \tag{6}$$

where

$$\begin{cases} \mathbf{x}(k) = [i_d, i_q]^T, \mathbf{u}(k) = [u_d, u_q]^T, v(k) = \psi_f, \\ \mathbf{A_c} = \begin{bmatrix} -RT_s/L_d + 1 & T_s\omega_e L_q/L_d \\ -T_s\omega_e L_d/L_q & -RT_s/L_q + 1 \end{bmatrix}, \\ \mathbf{B_c} = \begin{bmatrix} T_s/L_d & 0 \\ 0 & T_s/L_q \end{bmatrix}, \mathbf{C_c} = \begin{bmatrix} 1 & 0 \\ 0 & 1 \end{bmatrix}, \\ \mathbf{G}_c = [0, -\omega_e T_s/L_q]. \end{cases}$$

The cost function of the continuous-set MPC is designed as

$$\begin{aligned} \min_{\Delta \mathbf{u}_j} J_c(\mathbf{x}, \Delta\mathbf{u}_j) = \sum_{j=0}^{N_p-1} (\mathbf{x}_j^{ref} - \mathbf{x}_j)^T \mathbf{Q}_c (\mathbf{x}_j^{ref} - \mathbf{x}_j) + \\ \mathbf{x}_{N_p}^T T_c \mathbf{x}_{N_p} + \sum_{j=0}^{N_c-1} \Delta\mathbf{u}_j^{\mathbf{T}} \mathbf{R}_c \Delta\mathbf{u}_j \end{aligned} \tag{7}$$

$$s.t. \begin{cases} \Delta\mathbf{u}_j = \mathbf{u}_j - \mathbf{u}_{j-1} \\ \mathbf{x}_{min} \le \mathbf{x} \le \mathbf{x}_{max} \\ \mathbf{u}_{min} \le \mathbf{u} \le \mathbf{u}_{max} \end{cases}$$

where $\mathbf{Q_c}$, $\mathbf{T_c}$ and $\mathbf{R_c}$ are defined in Table I. Note that the optimization problem is ensured to be feasible through softening state constraints using slack variables. In this work, to compensate for control delays caused by digital implementation, a one-step state prediction is applied before calling the QP solver. Any standard QP solver can be used to solve this kind of quadratic programming with linear constraints.

B. Angle-based Repetitive Learning Observer

Based on the electromagnetic torque in (3), the cogging torque in (4) and the friction torque in (5), the dynamic equation describing torque ripple of QDD motors can be formulated as

$$J\ddot{\theta}_m = T_e - B\omega_m + T_d, \tag{8}$$

where the cogging and friction torques, as well as a pre-defined load T_l, are all incorporated into the disturbance term T_d as

$$T_d = -T_{cogg} - T_{fr} sign(\omega_m) - T_l. \tag{9}$$

Given that the cogging and friction torques both exhibit periodicity with respect to the motor angle, a period of N can be assumed. The term T_d can then be extended to N dimensions and expressed as

$$\mathbf{T}_d(k+1) = \mathbf{a}_{33}\mathbf{T}_d(k) \tag{10}$$

where $\mathbf{T_d}(k) = [\ T_{d1}(k) \quad T_{d2}(k) \quad \dots \quad T_{dN}(k)\ ]^T$, and

$$\mathbf{a}_{33} = \begin{bmatrix} 0 & 1 & 0 & \dots & 0 \\ 0 & 0 & 1 & \dots & 0 \\ \vdots & \vdots & \vdots & \ddots & \vdots \\ 0 & 0 & 0 & \dots & 1 \\ 1 & 0 & 0 & \dots & 0 \end{bmatrix}.$$

Let the observation of torque ripple at the moment k be denoted as $T_d(k) = T_{d1}(k)$, then

$$T_d(k) = \mathbf{C}_d \mathbf{T}_d(k) \tag{11}$$

where $\mathbf{C}_d = \begin{bmatrix} 1 & 0 & \dots & 0 \end{bmatrix}$.

To align with the period in (10), a full rotation of the motor's output shaft is also evenly divided into N partitions. This establishes a mapping between the time-based $T_d(k)$ and the corresponding motor angle to call the memorized torque ripple value by the algorithm, with the mapping index being determined as

$$i = \text{floor}\left[\frac{\theta_l(k)N}{2\pi}\right], i \in \{0, 1, ..., N-1\}. \tag{12}$$

Therefore, storage areas $\text{mem}_{\text{for}}[N]$ and $\text{mem}_{\text{rev}}[N]$, both with length of N, are allocated to store the torque ripple values in the forward and reverse directions, respectively. These torque ripple values are obtained online through the repetitive learning observer. Note that the greater the value of N, the higher the resolution of torque ripple, but it is also limited by the motor encoder resolution and the memory size of the microcontroller.

As mentioned in Section II-B, owing to the characteristics of the MPC current loop controller, the torque can quickly follow the desired value within a control cycle. Therefore, the desired torque $T_e^{ref}(k)$ of current cycle can be used as the torque measurement $T_e(k) = T_e^{ref}(k-1)$ of previous cycle, enabling the establishment of a state equation containing torque ripple as

$$\begin{cases} \mathbf{X}(k+1) = \mathbf{F}\mathbf{X}(k) + \mathbf{B}u(k), \\ y(k) = \mathbf{H}\mathbf{X}(k) \end{cases} \tag{13}$$

where

$$\begin{cases} \mathbf{X(k)} = \begin{bmatrix} T_e(k), & \omega_m(k), & \mathbf{T}_d(k) \end{bmatrix}^{\mathbf{T}}, \\ u(k) = T_e^{\text{ref}}(k), \\ \mathbf{B} = \begin{bmatrix} 1, & 0, & 0 \end{bmatrix}^{\mathbf{T}},\ \mathbf{H} = \begin{bmatrix} 0 & 1 & 0 \end{bmatrix}, \\ \mathbf{F} = \begin{bmatrix} 0 & 0 & 0 \\ a_{21} & a_{22} & a_{23}\mathbf{C}_d \\ 0 & 0 & \mathbf{a}_{33} \end{bmatrix}, \\ a_{21} = a_{23} = T_s/J,\ a_{22} = 1 - BT_s/J. \end{cases}$$

Based on (13), a repetitive learning observer can be constructed as

$$\hat{\mathbf{T}}_d(k+1) = \hat{\mathbf{a}}_{33}\hat{\mathbf{T}}_d(k) + \mathbf{L}a_{23}[T_d(k) - \hat{T}_{d1}(k)] \tag{14}$$

where $\hat{\mathbf{T}}_d(k) = \hat{\mathbf{T}}_d(k-N)$ is the torque ripple observation at time k, a forgetting factor Q is incorporated into $\hat{\mathbf{a}}_{33}$ as

$$\hat{\mathbf{a}}_{33} = \begin{bmatrix} 0 & 1 & 0 & \dots & 0 \\ 0 & 0 & 1 & \dots & 0 \\ \vdots & \vdots & \vdots & \ddots & \vdots \\ 0 & 0 & 0 & \dots & 1 \\ Q & 0 & 0 & \dots & 0 \end{bmatrix},$$

$\mathbf{L} = [L_1,\ L_2,\ ...,\ L_N]$ is a weight vector, and the torque ripple measurement is defined as

$$T_d(k) = \frac{\omega_m(k+1) - a_{21}T_e(k) - a_{22}\omega_m(k)}{a_{23}}.$$

Based on (10) and (14), the main performance parameters of the repetitive learning observer can be simplified to the forgetting factor Q and the weight coefficient L_N. The corresponding observation can be conducted as

$$\begin{aligned} \text{mem}_{\text{for}}[i]^{(k+1)} = Q\text{mem}_{\text{for}}[i]^{(k)} + \\ L_N a_{23}\{T_d(k) - \text{mem}_{\text{for}}[i]^{(k)}\} \end{aligned} \tag{15}$$

The details can be found in Algorithm 1. Note that to ensure the stability of the repetitive learning observer, the weight coefficient can be set according to

$$\begin{bmatrix} \mathbf{T}_d(k+1) \\ \hat{\mathbf{T}}_d(k+1) \end{bmatrix} = \begin{bmatrix} \hat{\mathbf{a}}_{33} & 0 \\ \mathbf{L}a_{23}\mathbf{C}_d & \hat{\mathbf{a}}_{33} - \mathbf{L}a_{23}\mathbf{C}_d \end{bmatrix} \begin{bmatrix} \mathbf{T}_d(k) \\ \hat{\mathbf{T}}_d(k) \end{bmatrix} \tag{16}$$

as

$$\det\left(\lambda\mathbf{I}_{2N} - \begin{bmatrix} \hat{\mathbf{a}}_{\mathbf{33}} & 0 \\ \mathbf{L}a_{23}\mathbf{C}_d & \hat{\mathbf{a}}_{33} - \mathbf{L}a_{23}\mathbf{C}_d \end{bmatrix}\right) = 0$$

$$\Rightarrow L_N = \frac{Q - \lambda^N}{a_{23}} \tag{17}$$

As a result, we set the range as $L_N a_{23} \in (Q-1, Q+1)$.

IV. EXPERIMENTS AND DISCUSSIONS

The simulation and experiments in this study have employed the same QDD motor parameters and controller parameters as shown in Table I. All simulations were conducted in MathWorks' Simulink software.

A. Experimental Setup

A set of real-world test rig was set up as shown in Fig. 3, where the left portion shows the motor testing platform for preliminary performance test of a single QDD motor and the right portion shows a two-degree-of-freedom robotic leg using two QDD motors at the same time. Each motor driver uses a digital signal processor TMS320F28379D from Texas Instruments, and the robotic leg is controlled by a master microcontroller STM32F767 through CAN communication with the motor driver. Note that a BOOSTXL-3PHGANINV GaN inverter is used in each QDD motor driver to improve its dynamic performance. The sampling frequency of the driver's current control loop is set to 20 kHz, while the motor's encoder resolution is 12 bit.

Algorithm 1 Angle-Based Repetitive Learning Observer

Update disturbance torque from flash storage to memory $\text{mem}_{\text{for}}[N]$ and $\text{mem}_{\text{rev}}[N]$
Measure encoder angle $\theta_l(k)$ at time t_k
while ARLO is online **do**
  Compute filtered speed $\omega_m(k)$
  Obtain $T_e(k) = T_e^{ref}(k-1)$
  Calculate angle mapping i from(12)
  if $i \neq i_{\text{prev}}$ **then**
    if forward rotation **then**
      Read last cycle's recorded $\hat{T}_d(k+1) = \text{mem}_{\text{for}}[i]$
      Update observed $\hat{T}_d(k+1)$ from(15)
      Record result into $\text{mem}_{\text{for}}[i]$
    else
      Read last cycle's recorded $\hat{T}_d(k+1) = \text{mem}_{\text{rev}}[i]$
      Update observed $\hat{T}_d(k+1)$ according to (15) by replacing $\text{mem}_{\text{for}}[i]$ with $\text{mem}_{\text{rev}}[i]$
      Record result into $\text{mem}_{\text{rev}}[i]$
    end if
  end if
  Update angle i to i_{prev}
  Predict next moment's QDD motor angle $\theta_l(k+1)$
  Calculate the output torque ripple suppression feed-forward information $\hat{T}_d(k+1)$ at $\theta_l(k+1)$
end while
Store from memory $\text{mem}_{\text{for}}[N]$ and $\text{mem}_{\text{rev}}[N]$ to flash

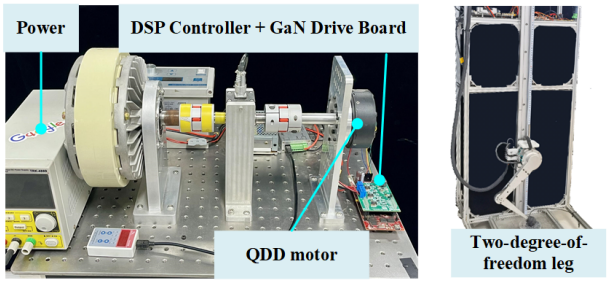

Fig. 3: The experimental setup for testing the proposed torque ripple reduction framework.

B. Simulation Results

Before conducting experimental verification, the performance improvement of MPC-based over PI-based current loop control is first checked in simulation.

1) Torque Bandwidth Enhancement Verification: The outer loop sampling frequency for both MPC-FOC and PI-FOC is 1kHz, with the inner loop sampling frequency for PI-FOC being 20kHz and for MPC-FOC being 5kHz. This longer interval is due to the computational burden of the optimization problem that must be solved at each iteration of MPC-FOC. The parameters of the MPC controller are shown in Table I. The corresponding solver was generated by the MATLAB's MPC toolbox and implemented in pure C language, involving only floating-point operations for optimized computation efficiency. To rigorously compare the performance of PI and MPC controllers, both methods were precisely tuned. Initially, the parameters of the QDD motor were identified through parameter estimation, with the results presented in Table I. The PI controller was designed following classical frequency response techniques for motor control systems [20]. The Modulus Optimum method was employed for the current controller to maximize closed-loop bandwidth, ensuring rapid response. The speed controller utilized the Symmetrical Optimum method to enhance stability and maximize phase margin, thereby improving robustness and disturbance rejection [21]. The MPC controller was designed based on the identified motor parameters and the state-space representation of speed-torque and current-voltage dynamics. The performance comparison of the PI and the MPC controllers is illustrated in Fig. 4.

It can be seen from Fig. 4 that despite MPC-FOC's inner loop sampling time is four times longer than that of PI-FOC, MPC-FOC's closed-loop performance surpasses PI-FOC. Specifically, MPC-FOC generates faster response and smaller overshoot in speed tracking. The quantitative performance comparison between MPC-FOC and PI-FOC can be found in Table II, where the proposed MPC-FOC shows an improvement of 25.7% in response time and 69.2% in overshoot.

TABLE I: Parameters

Motor parameters	Unit	Values
Stator phase resistance R	Ω	0.212
d-axis stator inductances L_d	H	$3.99 \cdot 10^{-5}$
q-axis stator inductances L_q	H	$6.32 \cdot 10^{-5}$
Magnet flux linkage ψ_f	Wb	$1.70 \cdot 10^{-3}$
Inertia$J$	$\text{Kg} \cdot \text{m}^2$	$1.68 \cdot 10^{-4}$
Rated current (phase-peak)	A	30
Friction Co-efficient	$\text{Kg} \cdot \text{m}^2/_s$	$9.21 \cdot 10^{-4}$
Number of pole pairs p	–	21
Gear Ratio N_{rat}	–	6:1
MPC parameters	**Unit**	**Values**
Prediction step N_p	–	2
Control step N_c	–	1
State matrix Q_c	–	[1 0;0 1]
Input matrix R_c	–	[0.01 0;0 0.01]
Terminal matrix T_c	–	[1 0;0 1]
ARLO parameters	**Unit**	**Values**
Forgetting factor Q	–	0.99
Weight coefficient $L_N a_{23}$	–	0.015
Storage area length N	–	4096

TABLE II: Speed tracking comparison.

Controllers	Response time[s]	Overshoot
PI-FOC	0.04405	19.60%
MPC-FOC	0.03750	6.04%
Improve	25.7%	69.2%

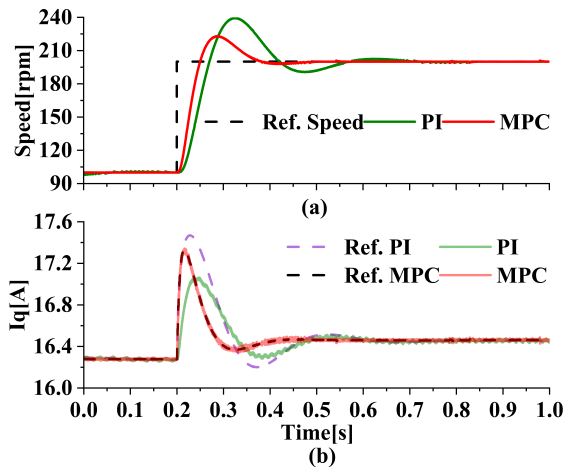

Fig. 4: Torque bandwidth enhancement verification. (a) Comparison of speed response waveforms between PI and MPC. (b) Comparison of torque tracking waveforms between PI and MPC.

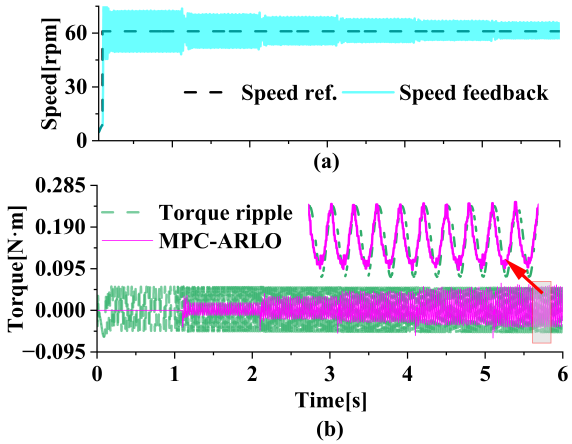

Fig. 5: Low reference speed with speed fluctuation rejection. (a) Speed reference and feedback. (b) The actual periodic torque ripple and the ARLO-observed torque ripple.

2) Torque Ripple Observation Verification: The effectiveness of the proposed ARLO method in observing periodic torque disturbances and suppressing torque ripple within the speed loop is also verified in simulation, including analysis of the speed fluctuation suppression waveform and the torque ripple observation waveform.

In applications with low inertiae and low speeds, periodic torque ripple due to the cogging and friction torques have a significant impact to motor speed, causing greater speed variation. Therefore, a simulation was conducted where the motor was set to rotate at a speed of 60 rpm under periodic torque ripple. The results show that, with ARLO activated, peak-to-peak speed fluctuation was significantly reduced by 72.7% after 6 seconds, as illustrated in Fig. 5(a). Fig. 5(b) demonstrates that ARLO progressively observed actual periodic torque ripple online.

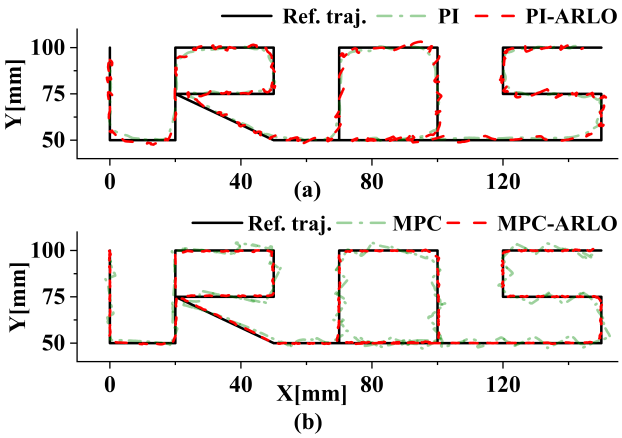

Fig. 6: Trajectory tracking of 'IROS'. (a) Comparison between PI with and without ARLO. (b) Comparison between MPC with and without ARLO.

C. Experimental Results

A two-degree-of-freedom robotic leg was set up to assess the effectiveness of the proposed method on torque ripple suppression. In this experiment, the leg's endpoint was commanded to follow an "IROS" trajectory to evaluate its tracking accuracy.

As illustrated in Fig. 6, the foot of the robotic leg using the proposed method in this paper gradually converged to the desired trajectory after several cycles, indicating that ARLO successfully observed and effectively suppressed the torque ripple from both QDD motors equipped. To further evaluate the performance improvement of MPC-FOC, the Root Mean Square Error (RMSE) between the reference and the actual trajectories was used to quantitatively analyze several methods together, the results of which are shown in the Table III.

TABLE III: Quantitative comparison of trajectory tracking performance.

Controllers	RMSE	Improvement
PI	7.86	–
PI_ARLO	6.97	11.3%
MPC	4.34	44.8%
MPC_ARLO	3.26	58.5%

It can be seen that the foot trajectory tracking RMSE with just PI-FOC was 7.86, which can be reduced to 6.97 when ARLO is added. For MPC-FOC, the RMSE was 4.34. superior to that of PI-FOC and even PI-ARLO. As with MPC-ARLO, the RMSE was further reduced to 3.26, which is a significant 58.5% reduction compared to the traditional PI-FOC controller, demonstrating enhanced smoothness of position control for QDD motors used in legged robots.

V. CONCLUSIONS

This paper proposes an online control method that simultaneously suppresses the cogging torque and the friction

torque and reduces the corresponding torque ripple in QDD motors, without the need for additional torque sensors in their robotic applications. In the speed control simulation, the proposed method has been able to suppress 72.7% of the speed fluctuation in QDD motors. In the motion control experiments with two QDD motors driving a robotic leg, the foot trajectory tracking RMSE has been reduced by 58.5%. These results show great potential of the proposed method in robotic applications using QDD motors. It can enhance smooth motion control and precise force control in scenarios where robust robotic motion is desired.

For the future work, we plan to further enhance the torque performance of QDD motors under high-load and high-speed conditions. The constraints of the MPC-based controller will be refined to achieve more aggressive motor utilization and more dynamic robotic motion. Additionally, the self-adaptive adjustment of ARLO parameters warrants further investigation for even more robust torque ripple suppression in QDD motors.

REFERENCES

[1] G. Bledt, M. J. Powell, B. Katz, J. Di Carlo, P. M. Wensing, and S. Kim, "Mit cheetah 3: Design and control of a robust, dynamic quadruped robot," in *2018 IEEE/RSJ International Conference on Intelligent Robots and Systems (IROS)*, 2018, pp. 2245–2252.

[2] D. V. Gealy, S. McKinley, B. Yi, P. Wu, P. R. Downey, G. Balke, A. Zhao, M. Guo, R. Thomasson, A. Sinclair, P. Cuellar, Z. McCarthy, and P. Abbeel, "Quasi-direct drive for low-cost compliant robotic manipulation," in *2019 international conference on robotics and automation (ICRA)*, 2019, pp. 437–443.

[3] P. M. Wensing, A. Wang, S. Seok, D. Otten, J. Lang, and S. Kim, "Proprioceptive actuator design in the mit cheetah: Impact mitigation and high-bandwidth physical interaction for dynamic legged robots," *IEEE Transactions on Robotics*, vol. 33, no. 3, pp. 509–522, 2017.

[4] T. Elery, S. Rezazadeh, C. Nesler, and R. D. Gregg, "Design and validation of a powered knee–ankle prosthesis with high-torque, low-impedance actuators," *IEEE Transactions on Robotics*, vol. 36, no. 6, pp. 1649–1668, 2020.

[5] M. G. Angle, J. H. Lang, J. L. Kirtley, S. Kim, and D. Otten, "Optimization of surface-mount permanent magnet synchronous machines for low duty-cycle, high-torque applications," in *2017 IEEE International Electric Machines and Drives Conference (IEMDC)*, 2017, pp. 1–6.

[6] M. Piccoli and M. Yim, "Anticogging: Torque ripple suppression, modeling, and parameter selection," *The International Journal of Robotics Research*, vol. 35, no. 1-3, pp. 148–160, 2016.

[7] B. G. Katz, "A low cost modular actuator for dynamic robots," Master's thesis, Massachusetts Institute of Technology, 2018.

[8] S.-H. Park, J.-C. Park, S.-W. Hwang, J.-H. Kim, H.-J. Park, and M.-S. Lim, "Suppression of torque ripple caused by misalignment of the gearbox by using harmonic current injection method," *IEEE/ASME Transactions on Mechatronics*, vol. 25, no. 4, pp. 1990–1999, 2020.

[9] M. G. Angle, J. H. Lang, J. L. Kirtley, S. Kim, and D. Otten, "Cogging torque reduction in permanent-magnet synchronous machines with skew," in *2016 XXII International Conference on Electrical Machines (ICEM)*, 2016, pp. 207–211.

[10] P. Bilancia, L. Monari, R. Raffaeli, M. Peruzzini, and M. Pellicciari, "Accurate transmission performance evaluation of servo-mechanisms for robots," *Robotics and Computer-Integrated Manufacturing*, vol. 78, p. 102400, 2022.

[11] M. S. Rafaq, W. Midgley, and T. Steffen, "A review of the state of the art of torque ripple minimization techniques for permanent magnet synchronous motors," *IEEE Transactions on Industrial Informatics*, vol. 20, no. 1, pp. 1019–1031, 2024.

[12] Z. Wang, J. Zhao, L. Wang, M. Li, and Y. Hu, "Combined vector resonant and active disturbance rejection control for pmslm current harmonic suppression," *IEEE Transactions on Industrial Informatics*, vol. 16, no. 9, pp. 5691–5702, 2020.

[13] M. G. Joksimovic, E. Levi, and S. N. Vukosavic, "Near-complete suppression of harmonic currents in spmsms caused by back emf and dead time," *IEEE Transactions on Industrial Electronics*, vol. 70, no. 5, pp. 4472–4484, 2023.

[14] M. J. Kim, F. Beck, C. Ott, and A. Albu-Schäffer, "Model-free friction observers for flexible joint robots with torque measurements," *IEEE Transactions on Robotics*, vol. 35, no. 6, pp. 1508–1515, 2019.

[15] M. Tang, A. Formentini, S. A. Odhano, and P. Zanchetta, "Torque ripple reduction of pmsms using a novel angle-based repetitive observer," *IEEE Transactions on Industrial Electronics*, vol. 67, no. 4, pp. 2689–2699, 2020.

[16] S. A. Q. Mohammed, H. H. Choi, and J.-W. Jung, "Improved iterative learning direct torque control for torque ripple minimization of surface-mounted permanent magnet synchronous motor drives," *IEEE Transactions on Industrial Informatics*, vol. 17, no. 11, pp. 7291–7303, 2021.

[17] M. Sumega, P. Rafajdus, and M. Stulrajter, "Current harmonics controller for reduction of acoustic noise, vibrations and torque ripple caused by cogging torque in pm motors under foc operation," *Energies*, vol. 13, no. 10, 2020.

[18] T. Li, X. Sun, G. Lei, Y. Guo, Z. Yang, and J. Zhu, "Finite-control-set model predictive control of permanent magnet synchronous motor drive systems—an overview," *IEEE/CAA Journal of Automatica Sinica*, vol. 9, no. 12, pp. 2087–2105, 2022.

[19] A. Brosch, O. Wallscheid, and J. Böcker, "Time-optimal model predictive control of permanent magnet synchronous motors considering current and torque constraints," *IEEE Transactions on Power Electronics*, vol. 38, no. 7, pp. 7945–7957, 2023.

[20] K. Ogata, *Modern Control Engineering*. Prentice Hall, 2010.

[21] *Motor Control Blockset: Getting Started Guide*, MathWorks, Natick, MA, USA, 2024, r2024a. [Online]. Available: https://www.mathworks.com/help/pdf_doc/mcb